X-RAY PROBES OF COSMIC STAR-FORMATION HISTORY

Pranab Ghosh[1,2] & Nicholas E. White[2]

[1] *Tata Institute of Fundamental Research, Bombay 400 005, India*

[2] *NASA Goddard Space Flight Center, Greenbelt, MD 20771*

ABSTRACT

In a previous paper (White and Ghosh 1998, WG98) we point out that the X-ray luminosity L_X of a galaxy is driven by the evolution of its X-ray binary population and that the profile of L_X with redshift can both serve as a diagnostic probe of the SFR profile and constrain evolutionary models for X-ray binaries. We update the WG98 work using a suite of more recently developed SFR profiles that span the currently plausible range. The first *Chandra* deep imaging results on L_X-evolution are beginning to probe the SFR profile of bright spirals and the early results are consistent with predictions based on current SFR models. Using these new SFR profiles the resolution of the "birthrate problem" of low-mass X-ray binaries (LMXBs) and recycled, millisecond pulsars in terms of an evolving global SFR is more complete. We also discuss the possible impact of the variations in the SFR profile of individual galaxies.

Subject headings: binaries: close–stars: formation–stars: evolution– galaxies: evolution–X-rays: galaxies–X-rays: stars

1. INTRODUCTION

Global star-formation rate (SFR) has undergone a strong cosmological evolution: it was larger than its present value by a factor ~ 10 at $z \approx 1$, had a peak value $\sim$ 10–100 times the present one in the redshift range $z \sim 1.5$–3.5, and declined again at high z (Madau *et al.* 1996; Madau, Pozzetti & Dickinson 1998, M98; Blain, Smail, Ivison & Kneib 1999, B99a; Blain *et al.*1999, B99b, and references therein). Details of the SFR at high redshifts are still somewhat uncertain, because much of the star formation at $2 \lesssim z \lesssim 5$ may be dust-obscured and so missed by optical surveys, but detected readily through the copious submillimeter emission from the dust heated by star formation (Hughes *et al.* 1998; Barger *et al.* 1999).

The X-ray emission of a normal galaxy (*i.e.*, one without an active nucleus) is dominated by the integrated emission of the galaxy's X-ray binary population (see *e.g.*Fabbiano 1995). In WG98 we discussed the basic effects of an evolving SFR on the evolution of X-ray binary populations of galaxies, and so on that of the total X-ray emission from normal galaxies. The X-ray luminosities L_X of normal galaxies should show significant evolution (up to a factor ~ 10, depending on the LMXB evolutionary timescale), even in the relatively nearby redshift range $z \sim 0.5$–1.0. In WG98 we also show that an evolving SFR can resolve the "birthrate problem" involving LMXB and their descendant "millisecond" radio pulsars (MRP, see Kulkarni & Narayan 1988; Lorimer 1995, L95).

The SFR profile used in WG98—the only profile available at the time—was based on the optical/UV data alone. Over the past 3 years there has been considerable progress in our understanding of cosmic star-formation history. In addition, very deep X-ray imaging with *Chandra* is beginning to detect normal galaxies in the redshift range $z \sim 0.5$–1.0, so that comparison with observations is becoming possible for the first time. In this *Letter*, we reconsider the key imprints left by the SFR evolution profile on the L_X-evolution profiles of normal galaxies, using the best SFR models currently available. We briefy discuss in this context the recent results of Brandt *et al.* (2001, Bran01) from the ultradeep *Chandra* imaging of the Hubble Deep Field North (HDF-N). A detailed calculation of the expected X-ray flux distribution of the HDF-N galaxies based on the results of this paper is reported by Ptak *et al.* (2001, P01). We also reconsider the resolution of the LMXB–MRP birthrate problem using the new SFR profiles.

2. X-RAY LUMINOSITY EVOLUTION WITH EVOLVING SFR

The total X-ray output of a normal galaxy can be modeled as the sum of those of its HMXB and LMXB wherein the evolution of each species "i" is described by a given timescale τ_i (see WG98). To study the effects of the dependence of τ_i on the binary period and other evolutionary parameters, we run the evolutionary scheme over ranges of likely values of τ_i suggested in the literature. The (prompt) evolution of the HMXB population in response to an evolving star-formation rate SFR(t) is given by

$$\frac{\partial n_{\rm HMXB}(t)}{\partial t} = \alpha_h {\rm SFR}(t) - \frac{n_{\rm HMXB}(t)}{\tau_{\rm HMXB}}, \qquad (1)$$

where $n_{\rm HMXB}$ is the number density of HMXBs in the galaxy, and $\tau_{\rm HMXB}$ is the HMXB evolution timescale. α_h is a coefficient representing the rate of formation of HMXBs per unit SFR, given approximately by $\alpha_h = \frac{1}{2} f_{\rm binary} f^h_{\rm prim} f^h_{\rm SN}$, where $f_{\rm binary}$ is the fraction of all stars in binaries, $f^h_{\rm prim}$ is that fraction of primordial binaries which has the correct range

of stellar masses and orbital periods for producing HMXBs (van den Heuvel 1992, vdH92 and the references therein), and $f_{\rm SN}^h \approx 1$ is that fraction of massive binaries which survives the first supernova. In the calculations reported here, we have adpoted a representative value $\tau_{\rm HMXB} \sim 5 \times 10^6$ yr according to current evolutionary models. Note that, in our introductory model here, $\tau_{\rm HMXB}$ includes both (a) the time of evolution of the massive companion ($\sim 4 - 6 \times 10^6$ yr) of the neutron star from the time of the supernova (that produces the neutron star) to the point where the "standard" HMXB phase begins, and, (b) the duration ($\sim 2.5 \times 10^4$ yr) of the HMXB phase (vdH92 and references therein). But since the second timescale is negligible compared to the first, little error is made by approximating this two-step process by a single-step one with an overall timescale $\tau_{\rm HMXB}$.

Two basic ways of producing LMXBs have been discussed. In the cores of dense globular clusters, they can be produced by the tidal capture of a neutron star by a normal star. Over the rest of a galaxy stellar densities are insufficient for tidal capture, and LMXBs are produced by the evolution of primordial binaries (see, *e.g.*, Webbink, Rappaport & Savonije 1983; Webbink 1992). In this paper, we consider only the latter mechanism. For spiral galaxies, at least, this must be the dominant mechanism, since the globular-cluster LMXB population in such galaxies only accounts for a relatively small fraction of the total X-ray luminosity.

The evolution of an LMXB from a primordial binary has two distinct stages (WG98), even after the supernova explosion that produces the neutron star in a post-supernova binary (PSNB). The PSNB first evolves on a timescale $\tau_{\rm PSNB}$ due to nuclear evolution of the neutron star's low-mass companion and/or orbital decay by gravitational radiation and magnetic braking, until the companion comes into Roche lobe contact and the LMXB turns on. The LMXB then evolves on a timescale $\tau_{\rm LMXB}$. Since $\tau_{\rm PSNB}$ and $\tau_{\rm LMXB}$ are comparable in general, we have to describe the two stages separately using a formulism similar to eqn 1 (see WG98 for more details).

We display evolution in terms of the redshift z, which is related to the cosmic time t by $t_9 = 13(z+1)^{-3/2}$, where t_9 is t in units of 10^9 yr, and a value of $H_0 = 50$ km s^{-1} Mpc^{-1} has been used. We consider the suite of current SFR models detailed in Table 1 to cover a plausible range, using the parameterization of B99a,b. Models of the "peak" class have the form

$$\mathrm{SFR}_{\rm peak}(z) = 2\left(1+\exp\frac{z}{z_{max}}\right)^{-1}(1+z)^{p+\frac{1}{3z_{max}}}, \qquad (2)$$

while those of the "anvil" class have the form

$$\mathrm{SFR}_{\rm anvil}(z) = \begin{cases} (1+z)^p, & z \le z_{max}, \\ (1+z_{max})^p, & z > z_{max}. \end{cases} \qquad (3)$$

These functional forms are not unique, but useful, since they have a convenient low-redshift limit, $\mathrm{SFR}(z) \propto (1+z)^p$, where all SFR profiles must agree with the low-z optical/UV data (M98), and the model parameters can be manipulated to mimic a wide range of star-formation histories (B99b). Peak-class profiles are useful for describing (a) SFRs determined from optical/UV observations, *i.e.*, Madau-type profiles (M98), (called "Peak-M" in Table 1) and, (b) more general SFRs with enhanced star formation at high z, a good example of which is a "hierarchical" model of B99b, wherein the submillimeter emission is associated with galaxy mergers in an hierarchical clustering model of galaxy evolution. Anvil-class profiles are useful for describing results of "monolithic" models. The "Gaussian" model (B99a,b) is an attempt at giving a good account of the SFR at both low and high z by making a composite of the Peak-G model (see Table 1) and a Gaussian starburst at a high redshift z_p, *i.e.*, a component

$$\mathrm{SFR}_{\mathrm{Gauss}}(z) = \Theta \exp\left\{-\frac{[t(z)-t(z_p)]^2}{2\sigma^2}\right\}. \tag{4}$$

This is based on the *IRAS* luminosity function, and is devised to account for the high-z data, particularly the submillimeter observations (B99a). For its parameters (see Table 1), we have used the revised values given in B99b. In all models considered here, no galaxies exist for sufficiently large redshifts $z > 10$.

Figures 1 and 2 show the evolution of HMXB and LMXB, as well as that of the total X-ray binary population (weighting the two components to represent the total X-ray emission from the galaxy). The LMXB profile peaks at redshifts $\sim$ 1–3 later than the HMXB profile, which is is a charcteristic signature of SFR evolution on the X-ray binary contents of galaxies (WG98). At low redshifts ($0 \lesssim z \lesssim 1$), the galaxy's X-ray emission is dominated by LMXBs, and at high redshifts, by HMXBs. As a result, the total L_X-profile is *strongly* influenced at high redshifts by the SFR profile, as Figure 1 shows.

Figure 1 compares the L_X-evolution corresponding to the (Madau or peak-M) SFR profile and the evolutionary timescales we originally used in WG98, *i.e.*, (a) $\tau_{\mathrm{PSNB}} = 1.9$ Gyr, $\tau_{\mathrm{LMXB}} = 0.1$ Gyr for the whole LMXB population, and (b) $\tau_{\mathrm{PSNB}} = 0.9$ Gyr, $\tau_{\mathrm{LMXB}} = 0.5$ Gyr for the short-period systems. In Figure 2, we display the L_X-evolution for a range of SFR profiles—Peak-M, Hierarchical, Anvil-10, and Gaussian, the evolutionary timescales being held fixed at $\tau_{\mathrm{PSNB}} = 1.9$ Gyr, $\tau_{\mathrm{LMXB}} = 1.0$ Gyr. Between them, the two figures thus explore the effects of (a) varying the evolutionary timescales for a fixed SFR profile, *viz.* Peak-M, and (b) varying the profile for a fixed set of evolutionary timescales.

Bran01 estimate that the average X-ray luminosity of the bright spiral galaxies at an average redshift $z \approx 0.5$ used in their stacking analysis is about a factor of 3 higher than in the local Universe ($z < 0.01$). This observed evolution, $L_X(0.5)/L_X(0.0) \sim 3$, can be

compared with the results in Table 2. The degree of evolution from $z = 0$ to $z = 0.5$–1.0 increases from Madau-type profiles to those with additional star formation at high redshifts, the numbers for the Peak-M profile being in best agreement with Bran01. More sophisticated estimates of the expected L_X-distribution of HDF-N galaxies, based on these evolutionary scenarios, are described in P01.

3. BIRTHRATE PROBLEM: FURTHER CONSIDERATIONS

As discussed in WG98 the evolution of MRPs from LMXBs involves the MRP number density $n_{\rm MRP}$, and evolution timescale $\tau_{\rm MRP} \sim 3\times10^9 - 3\times10^{10}$ yr (Camilo *et al.* 1994). Our evolutionary scheme yields the profiles of LMXB and MRP evolution for a given SFR profile, giving the number ratio, $N_r \equiv n_{\rm MRP}/n_{\rm LMXB}$, and the rate ratio, $R_r \equiv \frac{n_{\rm MRP}}{\tau_{\rm MRP}}/\frac{n_{\rm LMXB}}{\tau_{\rm LMXB}}$, of the MRP and LMXB populations at the present epoch ($z = 0$). We showed in WG98 that the Peak-M profile yielded $R_r \simeq 1$ for the overall MRP and LMXB populations, in agreement with current observations (L95). However, for short-period systems (LMXB periods $\lesssim 3$ day), this profile yielded a value $R_r \simeq 3$, smaller than the current value $R_r \approx 8$ estimated from observations (L95). On repeating these calculations with other SFR profiles which have large additonal star formations at high redshifts *e.g.*, the Gaussian and hierarchical profiles we now find reasonable agreement for both whole populations and short-period systems. These give $R_r \approx 6 - 8$ for short-period systems, for plausible evolutionary timescales.

A major new development in SFR research has been the first study of the star-formation histories of individual galaxies, and of galaxy-types. SFR profiles of individual galaxies, ranging from those in the Local Group to those in the HDF at redshifts $0.4 \lesssim z \lesssim 1$, have been inferred, using several different techniques (Glazebrook *et al.* 1999, Abraham *et al.* 2000, Hernandez *et al.* 2000). For individual galaxy-types, models of spectrophotometric evolution, which use the synthesis code *Pégase* and are constrained by deep galaxy counts (Rocca-Volmerange and Fioc 2000), leading to model SFR profiles. The birthrate problem was originally defined in terms of observations in our own galaxy and therefore we should use the SFR profile of our own galaxy. This profile is difficult to determine, as none of the above techniques is applicable to our own galaxy – but it may eventually be a tractable problem.

4. DISCUSSION

We have shown that different global SFR profiles within the currently admissible range lead to very different L_X-evolution profiles, so that the latter profiles can be an *independent*

diagnostic X-ray probe of cosmic star-formation history. The mechanism through which the SFR profile leaves its imprint is the interplay between the prompt evolution of HMXBs, which closely follows the SFR profile, and the slow evolution of LMXBs, which follow the SFR with a time lag of $\sim 10^9$ yr (WG98). Our results and a more detailed consideration by P01 show that the early *Chandra* results (Bran01) are consistent with the Peak-M profile, for LMXB evolution times ~ 1 Gyr.

We can clarify the *Chandra* results by applying the considerations of global and individual SFR profiles summarized in the last section. Bran01 used bright spirals for their stacking analysis. Rocca-Volmerange and Fioc (2000) have shown that the model SFR profile for such (Sa-Sbc) spirals rises roughly in a Madau fashion from $z = 0$ to $z \approx 1$ and thereafter flattens to a roughly constant value ~ 12 times that at $z = 0$, falling again at $z \gtrsim 7$. We can roughly represent this profile in the range $0 < z \lesssim 7$ by an anvil-type profile (see §2), with the parameter z_{max} as given in Table 1, and the parameter $p \approx 2.7$. On running our evolutionary scheme for such a profile with the timescales $\tau_{\rm PSNB} = 1.9$ Gyr, $\tau_{\rm LMXB} = 1.0$ Gyr, as in Figure 2, we get $L_X(0.5)/L_X(0.0) = 3.3$, and $L_X(1.0)/L_X(0.0) = 5.4$. This is in good agreement with both the Bran01 results and the Peak-M results summarized in §2, and so provides a natural explanation for why the Peak-M profile appears to give a good account of the Bran01 results. In effect, the Bran01 analysis may be probing the SFR profile of bright spirals in HDF-N. While the global analysis presented here is conceptually the most appropriate statistical descrption of a field like the HDF, we must be able to sample all types of galaxies in order to probe the global SFR observationally.

The X-ray probe considered here is a "fossil record" of SFR, as LMXBs preserve this record on a timescales ~ 1 Gyr. Conversely, as proving grounds for theories of X-ray binary evolution, this probe enjoyes a unique position, since such theories have been built almost wholly on the basis of our experience in the current epoch. This new probe provides a new means of watching LMXB evolution unfold over cosmic time.

It is a pleasure to thank L. Angelini, R. Griffiths, R. Mushotzky, and A. Ptak for stimulating discussions.

REFERENCES

Abraham, R. G., *et al.* 1999, MNRAS, 303, 641

Barger, A. J., *et al.* 1998, Nature, 394, 248

Blain, A. W., Smail, I., Ivison, R. J. & Kneib, J.-P. 1999, MNRAS, 302, 632 (B99a)

Blain, A. W., Jameson, A., Smail, I., Longair, M. S., Kneib, J.-P. & Ivison, R. J. 1999, MNRAS, 309, 715 (B99b)

Brandt, W. N. *et al.*, 2001, AJ, submitted [astro-ph/0102411] (Bran01)

Camilo, F., Thorsett, S.E. & Kulkarni, S.R. 1994, ApJ, 421, L15

Fabbiano, G. 1995, in X-ray Binaries, ed. W. H. G. Lewin, J. van Paradijs and E. P. J. van den Heuvel, p.390

Glazebrook, K., *et al.* 1999, MNRAS, 306, 843

Hernandez, X., Gilmore, G. & Valls-Gabaud, D. 2000, MNRAS, 317, 831

Hughes, D. H., *et al.* 1998, Nature, 394, 241

Kulkarni, S. & Narayan, R. 1988 ApJ, 335, 755

Lorimer, D. R. 1995, MNRAS, 274, 300 (L95)

Madau, P., Ferguson, H. C., Dickinson, M. E., Giavalisco, M., Steidel, C. C., & Fruchter, A. 1996, MNRAS, 283, 1388

Madau, P., Pozzetti, L., & Dickinson, M. 1998, ApJ, 498, 106 (M98)

Ptak, A. *et al.*, ApJ, submitted (P01)

Rocca-Volmerange, B. & Fioc, M. 2000, in Toward A New Millenium in Galaxy Morphology, ed. D. L. Block, I. Puerari, A. Stockton & D. Ferreira, Kluwer: Dordrecht [astro-ph/0001398]

van den Heuvel, E. P. J. 1992, in X-ray Binaries and Recycled Pulsars, ed. E. P. J. van den Heuvel and S. A. Rappaport, p.233 (vdH92)

Webbink, R. F. 1992, in X-ray Binaries and Recycled Pulsars, ed. E. P. J. van den Heuvel and S. A. Rappaport, p.269

Webbink, R. F., Rappaport, S., & Savonije, G. J. 1983, ApJ, 270, 678

Table 1: Star Formation Rate (SFR) Profiles[a]

Model	z_{max}	p	Comments
Peak-M	0.39	4.6	Madau profile
Hierarchical	0.73	4.8	Hierarchical clustering model[b]
Anvil-10	1.49	3.8	Monolithic models
Peak-G	0.63	3.9	"Peak" part of composite Gaussian
Gaussian	N/A	N/A	Gaussian starburst[c] added at high-z

[a]Model parameters taken from B99a,b.

[b]We have chosen the B99b model with a dust temperature 45 K. Note that the parameter p for the SFR equals 3/2 plus the value of the parameter p occurring in equation (16) for the merger efficiency in B99b.

[c]Parameters of Gaussian starburst component (see eq.[6] of text), are from the modified model given in B99b, *i.e.*, $z_p = 1.7$, $\sigma = 1.0$ Gyr, and $\Theta = 70$.

Table 2: Evolution of X-ray Luminosity L_X

Model	$\tau_{\rm PSNB}$	$\tau_{\rm LMXB}$	$\frac{L_X(0.5)}{L_X(0.0)}$	$\frac{L_X(1.0)}{L_X(0.0)}$
Peak-M	1.9	0.1	3.9	5.4
Peak-M	0.9	0.5	4.6	6.8
Peak-M	1.9	1.0	3.4	4.1
Hierarchical	1.9	1.0	6.2	11.3
Anvil-10	1.9	1.0	5.4	10.1
Gaussian	1.9	1.0	7.5	16.0

Fig. 1.— Evolution of HMXB population (dotted line), LMXB population (dash-dotted line), and the total X-ray luminosity L_X (solid line) of a galaxy with a given SFR (dashed line). As absolute ordinate scales are irrelevant for these evolutionary profiles, they have been adjusted for convenience of display: L_X always starts at 0.001 at $z = 0$, so that its evolution can be immediately read off the figure, and SFR always starts at 0.01 at $z = 0$, so that different SFR profiles can be readily compared. This figure is for the Peak-M profile (see text), showing the effect of varying the evolutionary timescales $\tau_{\rm PSNB}$ and $\tau_{\rm LMXB}$, whose values are written on each panel. The timescales used here are those used in WG98, corresponding to whole LMXB populations and short-period systems.

Fig. 2.— Same as Figure 1, but showing the effect of varying the SFR profile. The evolutionary timescales are kept fixed at $\tau_{\rm PSNB} = 1.9$ Gyr and $\tau_{\rm LMXB} = 1.0$ Gyr for all cases, and SFR profiles from Table 1 are used. Each panel is labeled by the name of its SFR profile. Evolutionary factors from this and the previous figure are collected in Table 2 and described in the text.

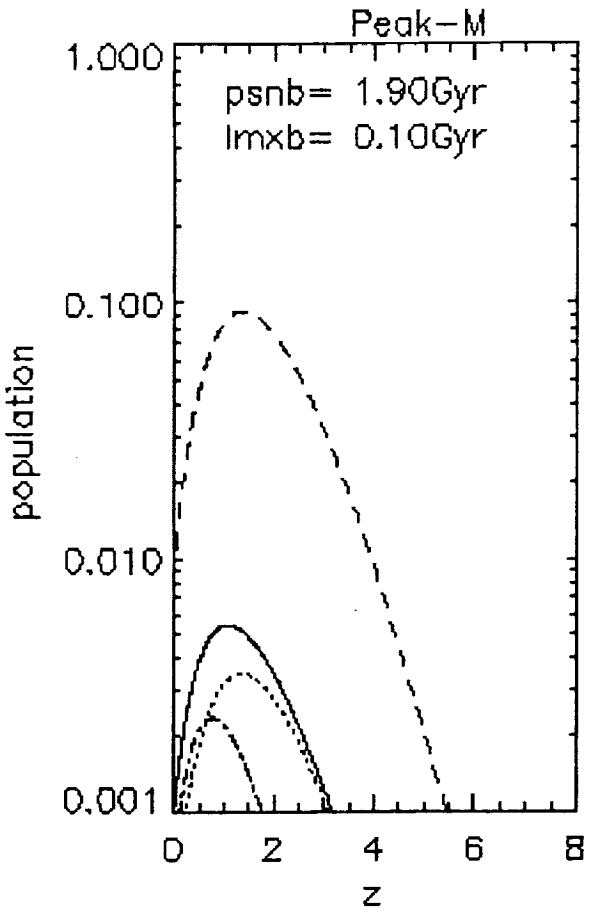
Peak−M
psnb= 1.90Gyr
lmxb= 0.10Gyr
1.000
0.100
0.010
0.001
population
0
2
4
6
8
z

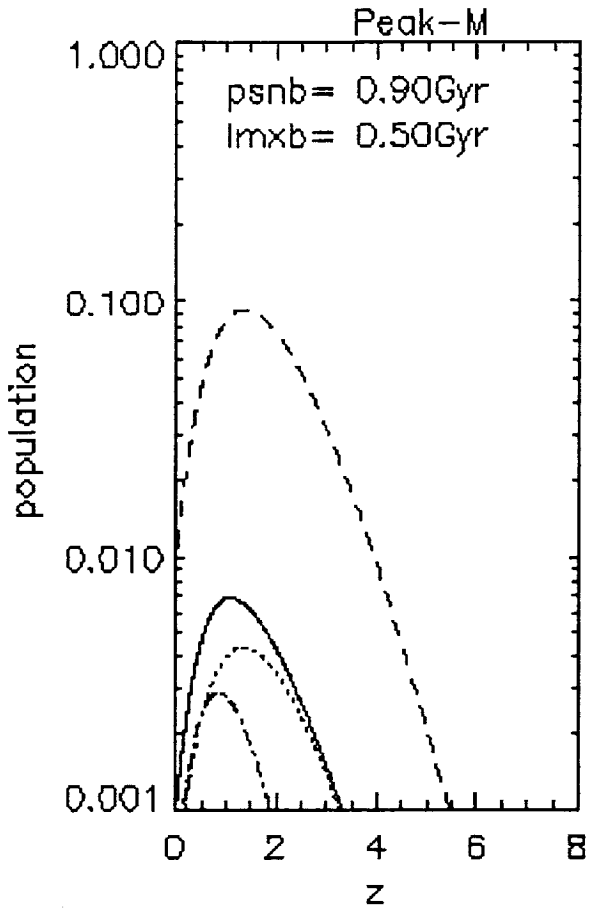
Peak−M
psnb= 0.90Gyr
lmxb= 0.50Gyr
1.000
0.100
0.010
0.001
population
0
2
4
6
8
z

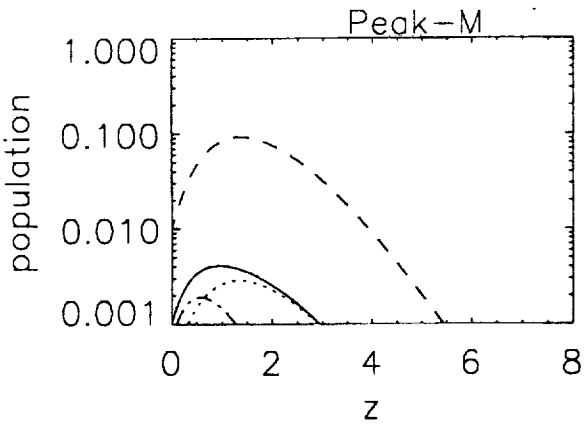
Peak−M
1.000
0.100
0.010
0.001
population
0
2
4
6
8
z

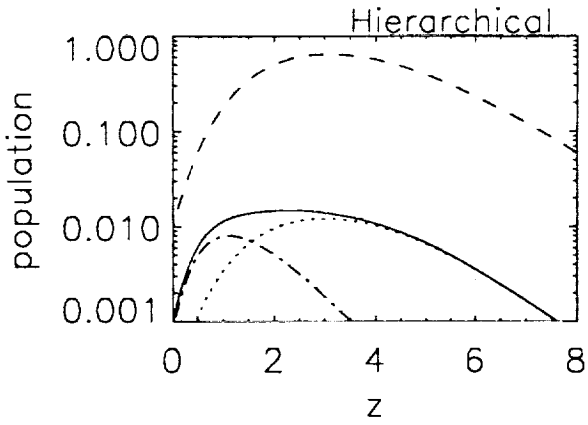
Hierarchical
1.000
0.100
0.010
0.001
population
0
2
4
6
8
z

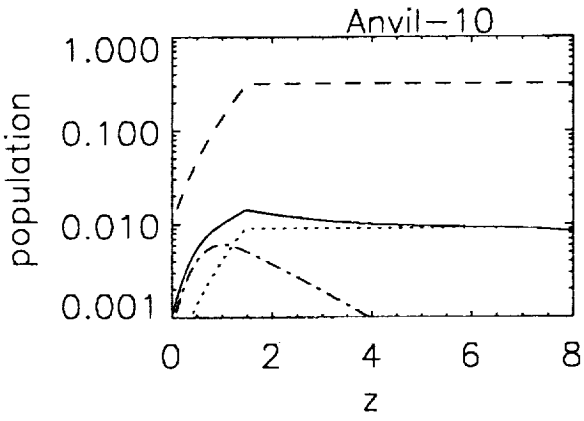
Anvil−10
1.000
0.100
0.010
0.001
population
0
2
4
6
8
z

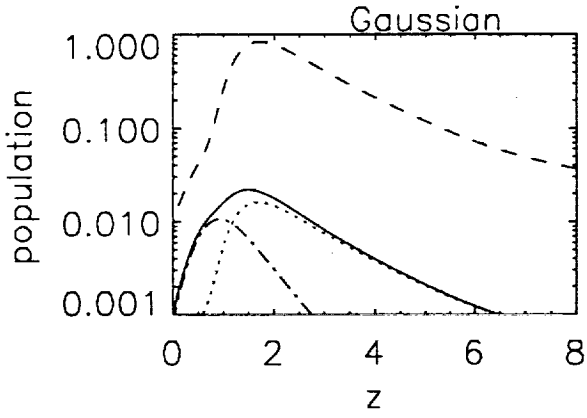
Gaussian
1.000
0.100
0.010
0.001
population
0
2
4
6
8
z